

FABRICATION OF SUPERHYDROPHOBIC POLYSTYRENE
SURFACES WITH TUNABLE ADHESION BY
MODULATING STRAIN RECOVERY TEMPERATURE

by

PRASHA SARWATE

Presented to the Faculty of the Graduate School of
The University of Texas at Arlington in Partial Fulfillment
of the Requirements
for the Degree of

Master of Science in Mechanical Engineering

THE UNIVERSITY OF TEXAS AT ARLINGTON

August 2014

Copyright © by Dr. Cheng Luo's Group 2014

All Rights Reserved



Acknowledgements

I would like to take this opportunity to extend my gratitude to my thesis adviser, my friends, colleagues and my family who helped me in successfully completing my degree work at UTA. I want to express immense gratitude to my thesis adviser Dr.Cheng Luo, his expertise in the field of micro/nano systems has been a constant source of knowledge, and his passion for research has been inspiring. He was tolerant, kind and supportive throughout the span of two years. I feel obliged to have received a chance of working with him. I want to thank my Thesis Committee members Dr.Hyejin Moon and Dr. Dennis DeSheng Meng, who took out time to be on the committee and to guide me.

I would like to extend my gratitude to Mingming Xiang for training me on various fabrication processes and for being patient with me during my starting days. I would also like to acknowledge the support of my group members Xin Heng, Lei Qiao and Anirban Chakroborthy during the progress of my thesis. I would like to thank the staff at Nanofab research centre, and at CCMB for training me on various fabrication and testing set ups. I would like to make a special mention of two very supportive staff members at the MAE department office, Debi Barton and Lannie Gordan.

I would like to thank my family, my mom, dad, brother, and my grandmother for their love and support through all the highs and lows. It was not always easy but your encouragement and unconditional support made things so much better. I would also like to remember my late grandparents whose blessings are always there with me.

I would like to extend my heartfelt gratitude to Varun Garg my best friend, confidant and colleague, for his unparalleled support and constant motivation. He has pushed me to do my best in everything and has always shown immense faith in me.

Finally, I would like to dedicate this thesis to my mother Mrs. Anu Sarwate and my father Mr. Shailendra Sarwate for all the hardships they went through to provide me with the best of everything and with the best educational opportunities.

June 20, 2014

Abstract

FABRICATION OF SUPERHYDROPHOBIC POLYSTYRENE SURFACES WITH TUNABLE ADHESION BY MODULATING STRAIN RECOVERY TEMPERATURE

Prasha Sarwate, M.S

The University of Texas at Arlington, 2014

Supervising Professor: Cheng Luo

In this work, different superhydrophobic structures were fabricated on the surfaces of polystyrene (PS) blocks, using oxygen reactive ion etch (ORIE) and controllable strain recovery. The PS used here is a thermal shape memory polymer (SMP). Microhills are first generated on the surface of a PS block by ORIE. The PS block is then heated up, which triggers the strain recovery. During this process of recovering its original shape, the PS block gradually reduces its lateral dimensions, while increasing its thickness. Using different recovery temperatures, the surface morphologies can be controlled, which provides an approach to adjust surface wetting properties, including adhesion.

At a temperature of 148 °C, microhills deformed to high-aspect-ratio nanowires. The corresponding PS surface has wetting properties similar to those of a lotus surface. The wetting is in Cassie-Baxter state, and a water drop is easy to get off from this surface. When the recovery temperature is increased to 162 °C, microwrinkles appear on the PS surface due to the different stiffnesses between the oxygen-treated top layer and the underlying PS substrate. These microwrinkles, together with nanowires located on their tops, form hybrid micro/nanostructures on the PS surface. The corresponding

surface has wetting properties similar to those of a rose petal. The wetting is in a mixed state of Wenzel and Cassie-Baxter. A water droplet is stuck on the surface, although its apparent contact angle is as high as $166^{\circ}\pm 2^{\circ}$.

Table of Contents

Acknowledgements	iii
Abstract	v
List of Illustrations	ix
List of Tables	xi
Chapter 1 Introduction.....	1
1.1 Definitions and Concepts.....	2
1.1.1 The Young- Dupre' Equation	2
1.1.2 Wenzel and Cassie Baxter Models of Wetting	3
1.2 Superhydrophobic Surfaces in Nature.....	5
1.3 Shape Memory Polymers	7
1.4 Thesis Outline.....	10
Chapter 2 Fabrication.....	11
2.1 Properties of PS Sheet	11
2.2 Procedure	13
2.3 Recovery Set-Up	14
Chapter 3 Surface Morphology	16
3.1. Dimensions and Surface Structures of Six Samples.....	16
3.2. Effect of ORIE on the PS Surface, and Formation of Biaxial Wrinkles	21
Chapter 4 Experimentation	23
4.1 Contact Angle Measurement	23
4.2 Tilt Tests	26
4.3 Roughness Factor Calculations.....	27
Chapter 5 Results and Discussions	29
5.1 Wetting States of Samples 1-5	29

5.2 Wetting on Sample 6	31
Chapter 6 Conclusions	34
References	36
Biographical Information	41

List of Illustrations

Figure 1-1:(a) A droplet resting on a solid surface with contact angle θ . (b) If the surface is rough, the liquid is in contact with irregularities, it is in Wenzel state.(c) If the liquid rests on the top of the irregularities, it is in Cassie Baxter state.[Image Source: Wikipedia, Superhydrophobe article]	5
Figure1-2:(a)Water droplet on a lotus petal,[Image Source: www.rsc.org] (b) SEM image of lotus surface, clearly showing the hierarchical structures covered with wax crystals. ...	5
Figure 1-3: (a, b) SEM images of the surface of a red rose petal, showing a periodic array of micropapillae and nanofolds on each papillae top. (c) Shape of a water droplet on the petal's surface, indicating its superhydrophobicity with a contact angle of 152.4° . (d) Shape of water on the petal's surface when it is turned upside down [10].	7
Figure 1-4: Integrated insight into SMPs based on structure, stimulus, and shape–memory function [18]......	9
Figure 2-1: Schematic diagram of the two step novel approach, of preparing the PS Film	12
Figure 2-2: Deformations of thin polystyrene films with the increase of temperature during the first recovery. The temperature was raised by a hot plate, and increased with time. The corresponding time taken for the hot plate to reach a certain temperature is beside the corresponding temperature [27]......	15
Figure 3-1: Schematics of the surface structures on Samples (a) 1, (b) 2, (c) 3, (d) 4, (e) 5 and (f) 6 (not to scale). x and y represent the width and height of a sample before the ORIE and heating.....	19
Figure 3-2: SEM images of surface structures on Samples (a) 1, (b) 2, (c) 3, (d) 4, (e) 5, and (f) 6.	20

Figure 3-3: SEM images of hybrid micro/nanostructures on the surface of Sample 6: (a) perspective and (b) close-up views..... 20

Figure 3-4: Changes in the dimensions of the six samples. (a) *y*-axis gives the temperature that each sample has experienced, (b) variation of thicknesses from Samples 1 to 6, (c) lengths and widths of Samples 1 to 6, and (d) average heights, distances between the peaks, and base diameters of microhills or nanowires from Samples 1 to 5. 21

Figure 4-1: Contact angles of water drops on the surfaces with an error of $\pm 2^\circ$: (a) untreated PS, (b) Sample 1, (c) Sample 2, (d) Sample 3, (e) Sample 4, (f) Sample 5 and (g) Sample 6..... 24

Figure 4-2: (a) A 10 μ L water drop still hanged on Sample 6 when this sample was rotated by 180°. (b) Time lapse image of a 10 μ L water droplet moving down the surface of Sample 5 at a tilt angle of 12°. 27

Figure 5-1: Optical images of Sample 6: (a) water filled valleys but not the top portions of the microwrinkles when a water drop was loaded on the sample surface and (b) addition of IPA to the water drop made the liquid also fill the top portions of the microwrinkles.... 31

Figure 5-2: Schematic of a mixed state of Wenzel and Cassie-Baxter. 32

Figure 5-3: Cross-sectional (SEM) view of a microwrinkle (the nanowires on the microwrinkle were not seen, since the focus of the SEM was on the microwrinkle). The inclination angle of the microwrinkle was measured to be $27^\circ \pm 1^\circ$ 33

List of Tables

Table 3-1: Dimensions of the samples.....	17
Table 4-1: Advancing contact angles, receding contact angles and contact angle measured experimentally, using an optical microscope.	25
Table 4-2: Values of r , f for sample 1-5 are tabulated.	28
Table 5-1: Values of intrinsic, experimental and theoretical contact angle for sample 1- 5.	30

Chapter 1

Introduction

The ability of some plants (such as lotuses) and insects (for example, butterflies) to repel water has interested researchers for several decades. The water-repelling nature is termed by scientists as superhydrophobicity, and, in contrast, water-loving nature is defined as superhydrophilicity. The plants that exhibit the capability to form spherical water drops on their leaves in rain, fog and dew are also called “self-cleaning.” The lotus leaf is a symbol of purity in many cultures, due to its ability to stay clean in muddy water. Hence, this self-cleaning behavior of lotus is popularly known as the lotus effect [1]. The leaf has hierarchical structures. Due to this, its surface exhibits a superhydrophobic behavior for water (the corresponding contact angle is above 150°). The high contact angle makes a small water drop have a spherical shape on a surface. Furthermore, the lotus surface has a low adhesion to water drops, enabling a water drop to easily roll off from this surface and taking away dusts. Researchers have been inspired by the lotus leaf to construct artificial surfaces with both superhydrophobicity and low adhesion by creating hybrid micro/nanostructures on flat surfaces [2-9].

In addition, it has been recently reported that a water drop can also form a contact angle above 150° on the surface of a rose petal [10]. The rose petal however exhibits high adhesion, instead of easy roll off. A water drop does not fall down from the surface, even if this surface is flipped over by 180° . The surface of a rose petal is densely distributed with micropapillae covered with nanofolds [10]. Motivated by petal effect, researchers have also developed artificial surfaces with both superhydrophobicity and high adhesion using roughness structures similar to those of a rose petal [11,12].

The artificial surfaces that have been constructed to date are designed to mimic either lotus or petal effect. On the other hand, little work has been done to produce artificial surfaces, which could be easily modified to have superhydrophobicity with tunable adhesion. Such surfaces may be applied to pin or repel water drops according to in-situ demands, thus providing more flexibility in applications. In this work, we have developed an approach to fabricate this type of surfaces using a thermal SMP. The following sub-sections include some basic concepts and the properties of SMPs.

1.1 Definitions and Concepts

Adhesive forces between a liquid and solid cause a liquid drop to spread across the surface. Cohesive forces within the liquid cause the drop to ball up and avoid contact with the surface. Contact Angle (CA) is determined by the resultant between adhesive and cohesive forces. Higher the CA less it wets the surface; hence it is an inverse measure of wettability [13]. Generally $CA < 90^\circ$ indicates favorable wetting of the surface and $CA > 90^\circ$ means that the wetting of the surface is unfavorable. So, for $CA > 90^\circ$ the fluid will minimize contact with the surface and forms a compact spherical liquid droplet.

Wetting can be understood by following some popular mathematical and thermodynamic theories and researchers in the past have developed methods and equation that explain the wetting phenomenon elaborately.

1.1.1 The Young- Dupre' Equation

The Young- Dupre' equation [14,15] dictates that neither γ_{SG} nor γ_{SL} can be larger than the sum of other 2 surface energies. This leads to predicting complete and zero wetting by following the two inequalities respectively:

$$\gamma_{SG} > \gamma_{SL} + \gamma_{LG}, \quad (1-1)$$

$$\gamma_{SL} > \gamma_{SG} + \gamma_{LG}. \quad (1-2)$$

The lack of a solution to the Young Dupre' equation is evidence that there is no equilibrium configuration with a CA 0° to 180° for those solutions. Another useful way of estimating wetting is S that is the spreading parameter [14,15].

$$S = \gamma_{SG} + \gamma_{LG}. \quad (1-3)$$

If $S > 0$, then liquid wets the surface completely. Otherwise, liquid may only wet the surface partially. The combination of spreading parameter definition with the Young relation yields the Young- Dupre' equation:

$$S = \gamma_{LG}(\cos \theta - 1), \quad (1-4)$$

which gives a relation between surface energy and contact angle.

1.1.2 Wenzel and Cassie Baxter Models of Wetting

Real surfaces are non-ideal in nature; they do not have perfect smoothness, rigidity or chemical heterogeneity. Ideal surfaces on the other hand are perfectly flat, smooth and thermodynamically stable. The deviation of real surfaces from ideality results in a phenomenon known as contact angle hysteresis (CAH). It is the difference between advancing (θ_a) contact angle and receding (θ_r) contact angle [11].

$$CAH = (\theta_a - \theta_r). \quad (1-5)$$

Cassie-Baxter and Wenzel state are the two main models that attempt to describe the wetting of rough textured surface. These equations only apply when the droplet size is sufficiently large as compared to the surface roughness scale [16].

The Wenzel Model was developed by R.N Wenzel in 1936 [16]. It describes the homogenous wetting regime, as seen in Figure 1-1(b). The following equation is suggested by this model:

$$\cos \theta_c = r \cos \theta. \quad (1-6)$$

In Eq (1-6) θ_c is the apparent CA, which refers to the state of stable equilibrium, r is the roughness ratio, and θ is the Young CA as defined for an ideal surface. In other words θ is the static CA on a flat surface.

Wenzel model is insufficient for heterogeneous surfaces. The Cassie-Baxter (CB) model was proposed by Cassie and Baxter [16]. This model deals with how the apparent CA changes when various materials are involved. It is a modification of the Cassie's Law, which describes how increasing roughness can increase the apparent contact angle. Its equation is as follows:

$$\cos \theta_c = f_1 \cos \theta_1 + f_2 \cos \theta_2, \quad (1-7)$$

Where θ_1 is the CA of the component 1 with surface area fraction as f_1 , and θ_2 is the CA of component 2 of the composite with surface area fraction as f_2 . If one component is air then $\theta_2 = 180^\circ$ and

$$\cos \theta_c = rf \cos \theta + f - 1. \quad (1-8)$$

In this equation r is the roughness ratio of the wet surface area, and f is the fraction of solid surface area wetted by liquid. When, it is a flat surface $f = 1$. Subsequently, eq. (1-8) becomes equal to Wenzel equation, i.e., eq. (1-6).

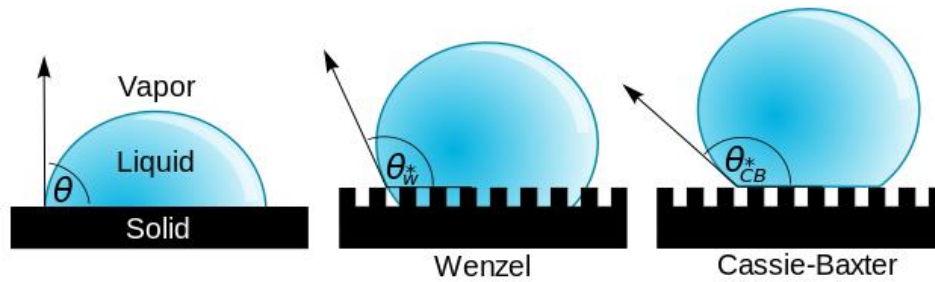


Figure 1-1:(a) A droplet resting on a solid surface with contact angle θ . (b) If the surface is rough, the liquid is in contact with irregularities, it is in Wenzel state.(c) If the liquid rests on the top of the irregularities, it is in Cassie Baxter state.[Image Source: Wikipedia, Superhydrophobe article]

1.2 Superhydrophobic Surfaces in Nature

Nature has been the inspiration for the development of superhydrophobic surfaces. It provides us with numerous examples of such surfaces. Some of them are lotus leaf, butterfly wings and insect feet. Lotus leaf is the most popular, as it grows in muddy water and stays clean, this is due to its inherent self-cleaning property. With development of better imaging techniques and analysis tools researchers now know that this behavior is due to the special hierarchical surface of the lotus leaf.



Figure1-2:(a)Water droplet on a lotus petal,[Image Source: www.rsc.org] (b) SEM image of lotus surface, clearly showing the hierarchical structures covered with wax crystals.

The lotus leaves have epidermal cells on their rough surface covered with wax crystals (Figure 1-2 (a)) [1]. The wax crystals provide a hydrophobic layer and the dual-size structure gives the surface high roughness. Therefore, water droplets on the surface are in the Cassie state, which means the water will roll over easily. On the other hand, contaminations on the surface are usually larger than the cellular structure of the leaves, leaving the particle resting on the tips of the surface structure. As a result, the contact area and thus the interfacial interactions are minimized. When a water droplet rolls over the contamination, dirt particles are adsorbed to the water droplet, and moved away from the surface as demonstrated in

Figure 1-2(b). This is the “lotus effect” and if replicated on other surfaces can result in self-cleaning materials [1]. Another type of superhydrophobicity as mentioned earlier takes place on rose petals Figure 1-2 (b)). The superhydrophobic rose petals exhibit high water droplet adhesion. The high-adhesive superhydrophobicity on red rose petal (*rosea* Rehd) was firstly characterized by Feng L et al [10], who reported that water droplets as large as 10 μl were able to remain on the petal surface when tilted upside down. It was suggested that the high adhesive force on the petal surface was due to a sort of combined wetting state between the Cassie and Wenzel states, where water was able to fill the large micrometer scale cavities on the rough surface, while the smaller cavities could entrap air and remain in the Cassie state, also known as Cassie impregnating wetting state. Researchers have divided opinion on the exact reason for this behavior of rose but the fact remains valid that this is also due to a hierarchical structure present on rose petal surface.

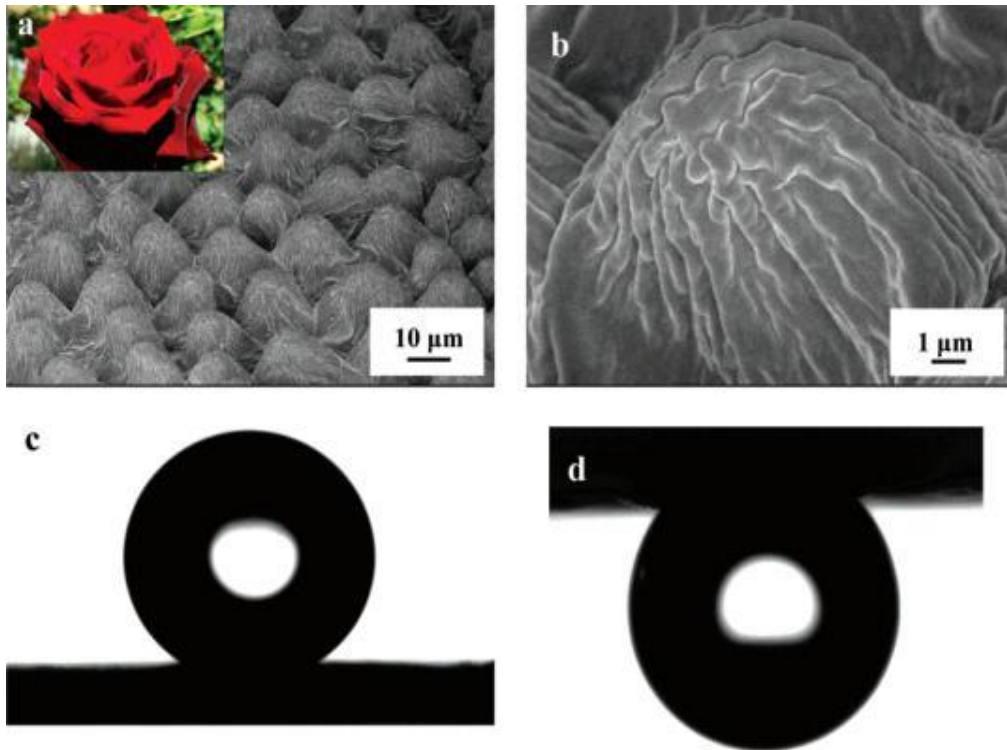


Figure 1-3: (a, b) SEM images of the surface of a red rose petal, showing a periodic array of micropapillae and nanofolds on each papillae top. (c) Shape of a water droplet on the petal's surface, indicating its superhydrophobicity with a contact angle of 152.4° . (d) Shape of water on the petal's surface when it is turned upside down [10].

1.3 Shape Memory Polymers

SMPs are a category of smart materials that offer mechanical action triggered by an external stimulus. The abilities of SMPs to fix a temporary shape and also to recover an original shape in a controlled fashion through use of external stimuli (i.e., heat, electric field, and irradiation) distinguish them from conventional polymers [18].

SMPs have several advantages like; they can use diverse external stimuli in addition to heating to trigger shape recovery, they exhibit high level of flexibility

programming, they have a large range of structural designs, they may possess tunable properties by using composites and different synthesis materials, they are biodegradable and they can be very light and can occupy a large volume. These properties make them important for a wide range of applications from smart biomedical devices to aerospace applications [18]. The driving force for strain recovery for strain recovery in SMPs is the entropic elasticity of the polymer network. In the field of micro- and nanotechnology, SMPs have been applied, for example, to fabricate high-aspect-ratio micropillars [20,21], microfluidic channels[22], microreservoirs [23], nanowrinkles [24-26] and sidewall patterns [27-29].

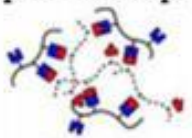
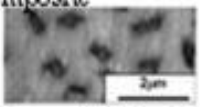
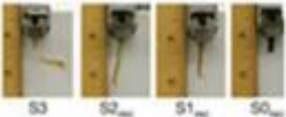
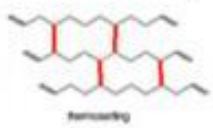
Composition & structure	Stimulus	Shape memory function
Block-copolymer 	Temperature 	One way SME 
Supramolecular polymer 	Electricity 	Two way SME 
Polymer blend / composite 	Magnetic 	Tiple shape SME 
Polymer IPN/semi IPN 	Water sensitive 	Multi shape SME 
Crosslinked Homopolymer 	Light/radiation 	Multi functionality 
	Oxidation-reduction 	
	1) Thermal sensitive 2) Water sensitive 3) Light sensitive 4) Redox sensitive	

Figure 1-4: Integrated insight into SMPs based on structure, stimulus, and shape-memory function [18].

When a rigid film supported on a soft substrate is compressed laterally beyond a critical strain, the mechanical instability leads to surface wrinkling. The moduli of SMPs at temperature above shape-memory transition temperature are in line with the elastomers, the SMPs are popularly used as wrinkle substrate. Researchers have been working with creating local indent [18], different patterns of self-organized wrinkles are obtained atop PS SMPs [26] etc.

1.4 Thesis Outline

In this thesis work we have used the above mentioned concepts and special qualities of SMPs to fabricate various types of surface roughness that exhibit tunability in their wetting characteristics. All the surfaces created in this work are superhydrophobic but with variable adhesion. The following chapters will include the detailed fabrication techniques, surface morphology details, formation of biaxial wrinkles, surface wetting properties, experimental results and discussions and conclusion.

The motivation to pursue this work has come from our groups past work and the vast possibility of application that this modified PS film may have in the future. The ease of fabrication and variation in wetting from hydrophilic to superhydrophobic in Cassie Baxter state, and then to a special state that increases adhesion enormously has been very interesting to investigate.

Chapter 2

Fabrication

The fabrication for our required type of surfaces is facile, convenient and efficient. It is a two-step process and has proved quite efficient in remaking the samples multiple times. It is also similar to the procedures adopted by our group to generate microchannels in a PS film [28,29].

2.1 Properties of PS Sheet

In this work we have used the PS sheet which is a commercial packaging product (Multi Plastics Inc.). This sheet is biaxially oriented polystyrene and is widely used in packaging applications. The orientation of the polymer improves the mechanical properties in comparison to the unoriented polymer. The sheets are processed by heating the polystyrene to a temperature that is a few degrees below the glass transition temperature and then hot stretching the sheet into a film. The polymer chains are entangled and have highly extended conformations in the plane of the film post processing [20]. During relaxation the polymer chains reorganize themselves to their undisturbed conformations. Heating the polymer above its glass transition temperature (T_g) accelerates relaxation, this results in reorganization due to which the film shrinks in plane of the film and its thickness increases. This is the reason it is called a thermal SMP, and has capability to recover from its deformed shape to original shape upon heating above its T_g .

The PS was specifically adopted in this work due to two reasons. First, it has shown the capability of having the largest strain recovery (i.e., 2,000% [20, 21]) among the SMPs. Second, this material was a thermal SMP, and only needed heating to recover its large strain levels. According to Ref. [20] and [21], the PS had been processed into

the present form by the manufacturer by heating a PS sheet to a temperature a few degrees below T_g and stretching the sheet into a 30- μm -thick film along two perpendicular directions to form a film. The degree of shrinkage is approximately equal to the draw ratio of the orientation process. The T_g and melting temperature of the sheet were 95 °C and 270 °C, respectively. The PS sheet was received from the manufacturer in stretched form and recovery will shrink it to its natural form.

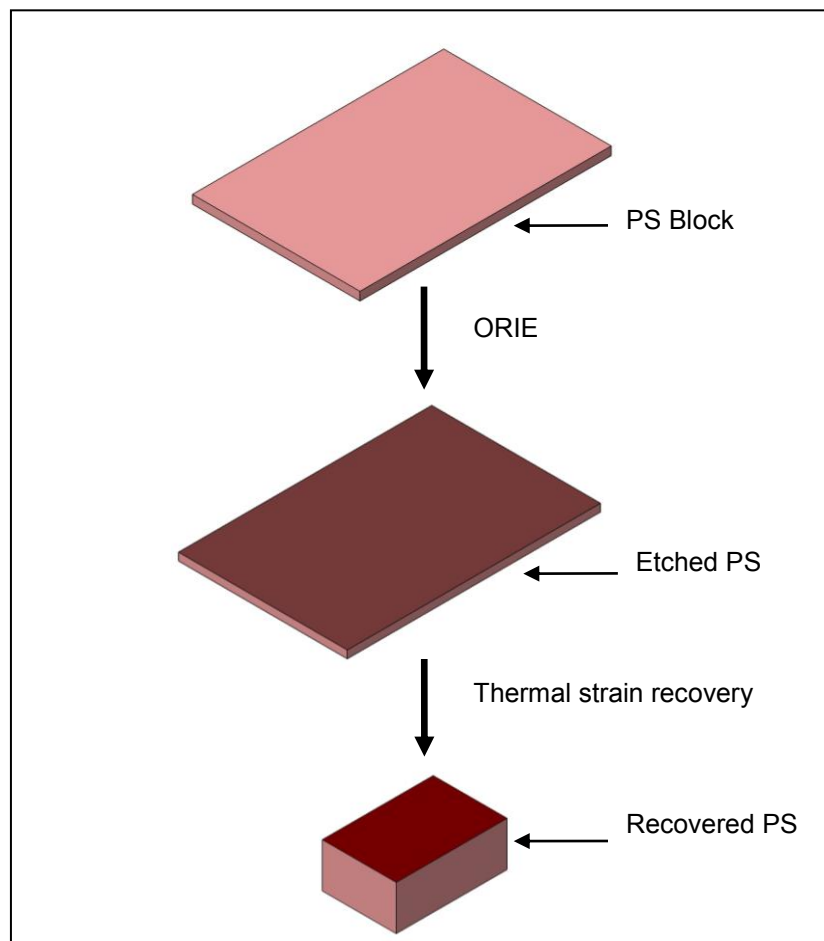


Figure 2-1: Schematic diagram of the two step novel approach, of preparing the PS Film

2.2 Procedure

The process of generating hybrid micro/nanostructures using the strain-recovery property of polystyrene (PS) is divided into two simple steps (Figure 2-1):

- The treatment of the surface of a PS sample using ORIE.
- The strain recovery of this PS sample by heating it above T_g .

In the first step of fabrication, six identical blocks with dimensions of 3 cm x 2 cm x 30 μm (length x width x thickness) were first cut from a PS sheet, and then cleaned with isopropyl alcohol (IPA) and de-ionized water. Then, they were kept in the ORIE set up. The ORIE was conducted in a commercial machine (Model: Plasma Lab RIE, Plasma Technology Inc., Torrance, CA, USA). The radio frequency power was maintained at 150 W, the pressure was maintained between 170 to 180 mTorr, and oxygen flow rate was fixed at 11.25 standard cubic centimeters per minute. The total etch time was in the range of 90 to 100 min. The approximate etch rate was found to be 0.1 $\mu\text{m}/\text{min}$.

Our group has used the ORIE technique to generate microchannels in a PS film [28,29], as well as to remove undesired poly(methyl methacrylate) films [30]. After the ORIE, the surface structures of a PS block, which is, for simplicity, called Sample 1 thereafter, were examined using a scanning-electron microscope (SEM).

In the second step, the remaining five PS blocks that had been treated with the ORIE were heated at different temperatures for strain recovery. In addition to T_g , another three temperatures are also important in the thermo-mechanical response of a thermal SMP[18] T_s , T_d , and T_r , they stand for temperatures of storage, initial deformation, and strain recovery, respectively. In our previous work [27], the corresponding T_s , T_d , and T_r used for as-received PS blocks were 20 °C, 120 °C, and 160 °C, respectively. Using these temperatures as reference, the five PS blocks were recovered on a hot plate, respectively, at 93°C, 107°C, 121 °C, 148°C and 162 °C to characterize the deformations

at different temperatures. These five samples are referred to as Samples 2 to 6 thereafter.

2.3 Recovery Set-Up

Teflon-coated glass slides were used as the substrates for the PS blocks. Each glass slide was 75 mm long, 25 mm wide and 1 mm thick (Fisher Scientific Co., Waltham, MA, USA). Teflon is a material of low surface energy. It was coated on the glass substrate to avoid the adhesion between a PS block and its glass substrate during the strain recovery. As discussed earlier from Refs. [20, 21], the bending configurations that were observed during the recovery process are in accordance with the fact that PS film is stretched over the cylindrical roller by the manufacturer. As observed in previous work by our group [27], the PS block was not flat until the temperature reached 120 °C in this process. To keep every heated sample flat to examine its wetting properties, which will be addressed in Sub-sections 3.4 and 3.5, different from what was done in our previous works [27-29], a Teflon-coated glass slide was also put on the top of each sample during the recovery process. The two glass slides were fixed between a pair of tweezers, and the gap between the two glass slides was 440 μm .

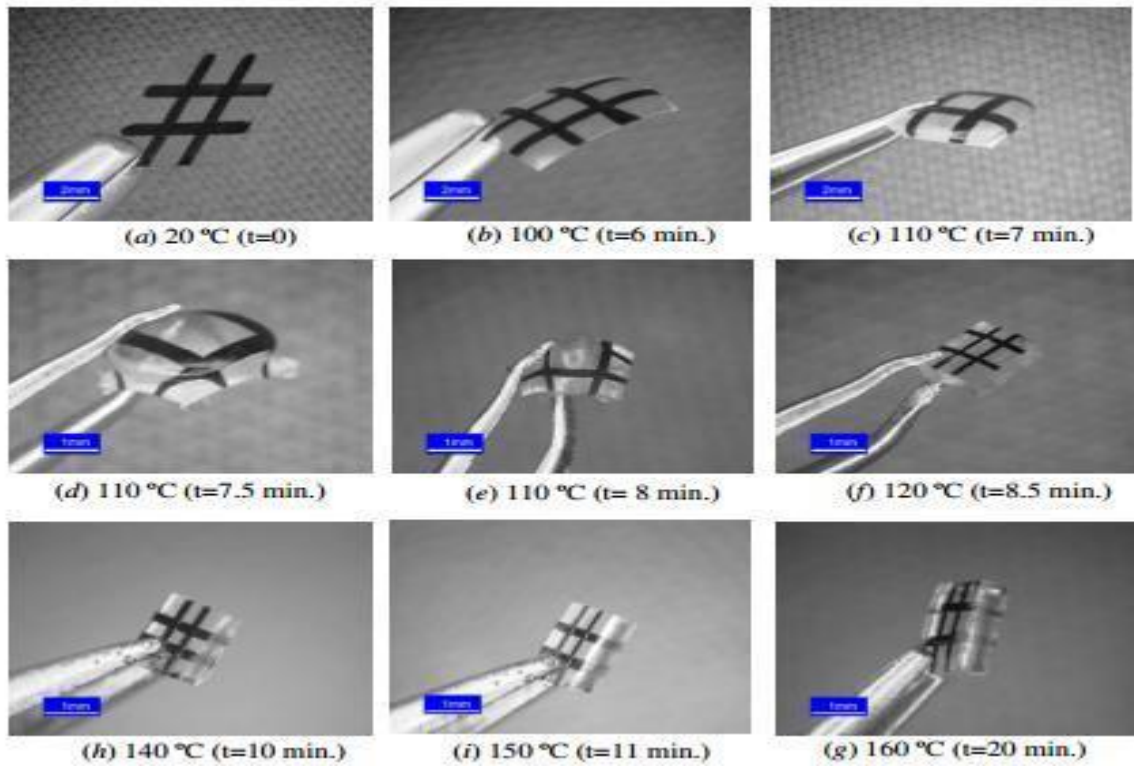


Figure 2-2: Deformations of thin polystyrene films with the increase of temperature during the first recovery. The temperature was raised by a hot plate, and increased with time. The corresponding time taken for the hot plate to reach a certain temperature is beside the corresponding temperature [27].

Chapter 3

Surface Morphology

The six samples were tested for their morphology analysis by the use of SEM. The structures atop all the samples were measured carefully and are reported in this section. The morphology plays a key role in wetting properties of the samples. The methods used were SEM imaging, digital measuring software MB-Ruler, and optical microscope.

3.1. Dimensions and Surface Structures of Six Samples

Due to varying recovery temperatures, it was expected that we will notice changes on the surface structures; the 6 samples were hence analyzed using a SEM set up. Figure 3-1 illustrates the surface morphology variations produced during fabrication schematically. The height and the average value of the two lateral dimensions of each sample are also marked in this figure. SEM results are given in Figure 3-2-Figure 3-3. The two points observed from the results are described as follows.

Firstly, surface morphology varies for each sample. During the ORIE process cylindrical microhills with base diameters of 1.5 μm , average height of 0.75 μm and peak-peak distance of 1.7 μm were formed on the substrates due to the bombardment of the oxygen ions to the surface (Figure 3-1(a) and Figure 3-2(a)). When the temperature was increased to 148 $^{\circ}\text{C}$ i.e sample 5, due to the strain-recovery deformations of the PS, the microhills gradually shrank, becoming high-aspect-ratio nanowires with an average diameter and height of 450 nm and 2.4 μm , respectively (Figure 3-1(e) and Figure 3-2(e)). Meanwhile, the valleys between the microhills became deeper and narrower, and the distance between two neighboring nanowires was 320 nm. At 162 $^{\circ}\text{C}$ i.e sample 6, wave-like microwrinkles appeared (Figure 3-1(f) and Figure 3-2(f)). On average, these

wrinkles were 2.3 μm high, 7.8 μm wide, and the peak-to-peak distance between two neighboring wrinkles was 8.3 μm . The wrinkles bear nanowires on top with average height of 1.3 μm , width of 400 nm, and distance of 200 nm between nanowires (Figure 3-3). Accordingly, hybrid micro/nano structures were formed on the surface while only microhills or nanowires were constructed on the surfaces of the other five samples. Meanwhile, nanowires were not observed on the valleys between the microwrinkles on Sample 6 (Figure 3-1(f)).

Secondly, the six samples have different dimensions (Table 3-1 and Figure 3-1, Figure 3-2 & Figure 3-4). As expected, the thicknesses, widths and heights gradually changed from Samples 1 to 3, while they had greater changes from Samples 4 to 6 (Figure 3-1), since the heating temperatures of the latter three samples were above T_d . For example, the thicknesses of Samples 1, 3 and 6 are 20, 35, and 440 μm , respectively. The comparison of Sample 6 with Sample 1 indicates that, at 162 $^{\circ}\text{C}$, the shrinkage of the PS reduced lengths and widths of the block by factors of 4.3 and 5.0, respectively, and increased the height (thickness) by a factor of 22.0 (Figure 3-1 and Figure 3-4). On the other hand, in our previous tests on an as-received PS block which did not receive any ORIE treatment, the recovered PS reduced two lateral dimensions of the block by factors of 3.6 and 5.7, separately, and increased the height by a factor of about 25 [27].

Table 3-1: Dimensions of the samples

Sample No.	Temp($^{\circ}\text{C}$)	Thickness(μm)	Length(mm)	Width(mm)
1	24	20	30	20
2	93	25	28.5	20
3	107	35	24	18
4	121	85	21	12
5	148	320	8	4.4
6	162	440	7	4

Two points were observed from the differences in the deformation degrees:

- First the creation of microcavities on the top surface of a PS sample using the ORIE did not cause dramatic changes in the lateral dimensions, probably due to the fact that the microcavities were not deep enough in comparison with the thickness.
- Second the thickness of Sample 6 was equal to the gap of the two glass slides, indicating the reduction in the recovery degree along the vertical direction was caused by the constraint of the top glass slide.

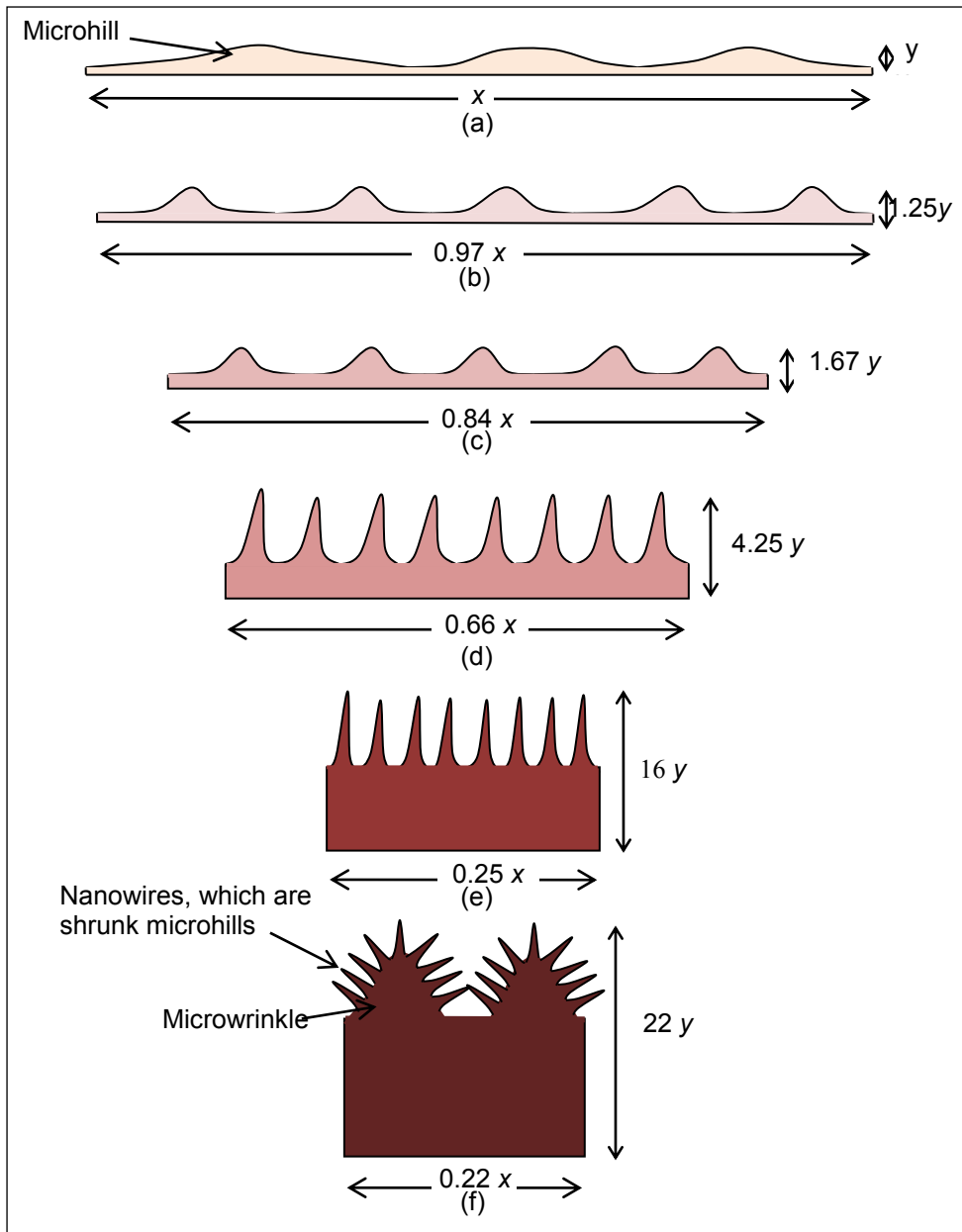


Figure 3-1: Schematics of the surface structures on Samples (a) 1, (b) 2, (c) 3, (d) 4, (e) 5 and (f) 6 (not to scale). x and y represent the width and height of a sample before the ORIE and heating.

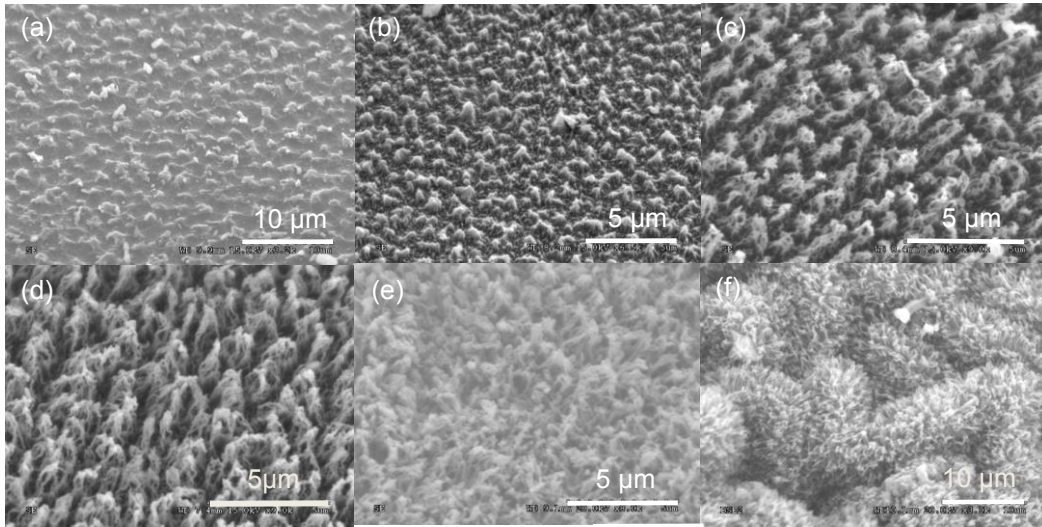


Figure 3-2: SEM images of surface structures on Samples (a) 1, (b) 2, (c) 3, (d) 4, (e) 5, and (f) 6.

Sample 6 showed clear wrinkling of the surface due to the difference between hardness of the top plasma treated surface, discussed in detail in the next sub-section. The clearer image for this sample is shown in Figure 3-3; a clear demarcation between valleys and nanowires covered microwrinkles can be seen.

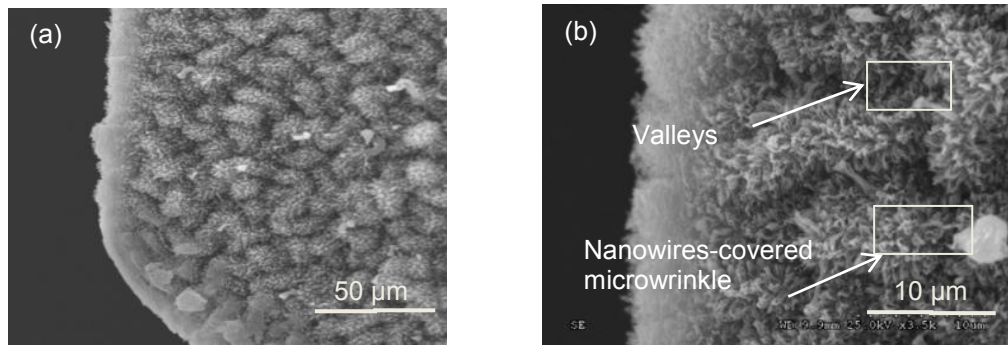
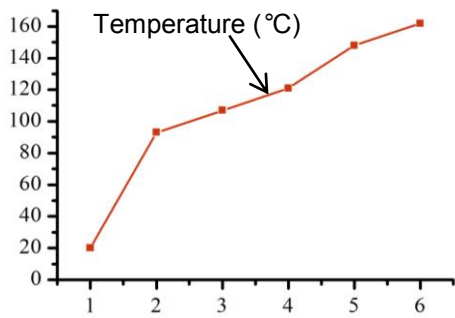
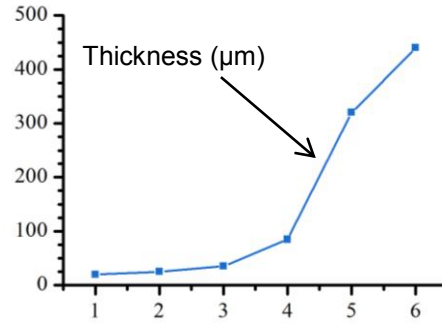


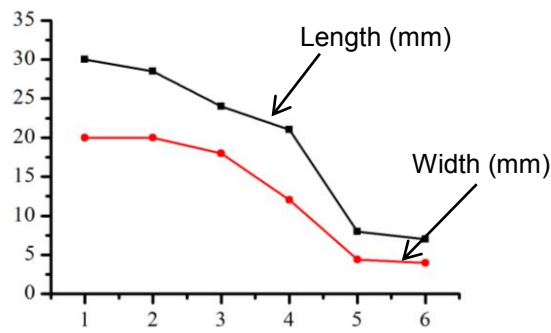
Figure 3-3: SEM images of hybrid micro/nanostructures on the surface of Sample 6: (a) perspective and (b) close-up views



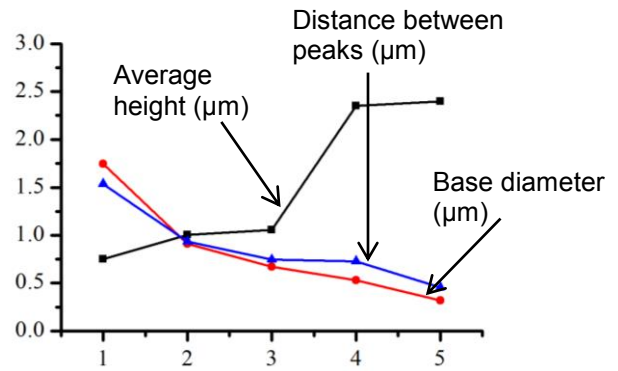
(a)



(b)



Sample No.
(c)



Sample No.
(d)

Figure 3-4: Changes in the dimensions of the six samples. (a) *y*-axis gives the temperature that each sample has experienced, (b) variation of thicknesses from Samples 1 to 6, (c) lengths and widths of Samples 1 to 6, and (d) average heights, distances between the peaks, and base diameters of microhills or nanowires from Samples 1 to 5.

3.2. Effect of ORIE on the PS Surface, and Formation of Biaxial Wrinkles

During the ORIE treatment of the PS, two processes occur: (i) etch of the polymer surface due to formation of volatile by-product of the reaction between atomic oxygen and surface carbon atoms, When the polymer is treated with inert gas plasma,

the low molecular weight chains on the surface are detached and this improves the cross linkage density hence the surface is activated [31]. This resulting in the formation of the surface observed in Figure 3-1(a); and (ii) It is widely known that an oxygen plasma can react with the polymer surface to produce a variety of atomic oxygen functional groups including C-O, C=O, O-C=O and CO₃ on the PS surface[32], yielding a hard oxide layer on this PS surface [31]. A similar oxide skin formation in polydimethylsiloxane (PDMS) has been previously reported by other researchers [33].

If a stiff thin film attached to a soft substrate is subjected to stress, it is likely that the stress is relieved by wrinkling of the thin film [34]. Wrinkles were found in Au films when their PDMS [35] and PS substrates shrank [24]. The critical wavelength of biaxial wrinkles, λ_c , and the critical compressive strain, ϵ_c , are defined as [26]:

$$\lambda_c = 2\pi h \left[\frac{4E_s(1-\nu_p^2)}{3E_p(1-\nu_s^2)} \right]^{1/3}, \quad (3-1)$$

$$\epsilon_c = \left[\frac{3E_p(1-\nu_m^2)}{4E_s(1-\nu_p^2)} \right]^{2/3}, \quad (3-2)$$

where E_s and ν_s are, respectively, Young's modulus and Poisson's ratio of the oxide layer, E_p and ν_p are those of the bulk PS, and h is the thickness of the oxide layer.

It follows from these two equations that λ_c and ϵ_c are related as

$$\lambda_c = \frac{2\pi h}{\sqrt{\epsilon_c}} \quad . \quad (3-3)$$

The average λ of the wrinkles observed was 8.3 μm and the average ϵ_c may be estimated as the average lateral shrinkage of the microstructures on top of the PS film during strain-recovery which was 0.7. From Eq. (3.3), h is calculated to be 2.1 μm , indicating that the thickness of the oxide layer is in the order of 1 μm .

Chapter 4

Experimentation

As discussed in the introduction chapter, we understand that the surface wetting can be characterized by the surface roughness, contact angle and contact angle hysteresis. The experiments were carefully chosen in order to deal with each sample, to efficiently predict and confirm its wetting properties later.

4.1 Contact Angle Measurement

The wetting properties of the six samples were examined. For the purpose of comparison, the same wetting tests were performed on an untreated PS block, which was also cut from the same PS sheet and experienced neither ORIE nor strain-recovery process, this sample was called as untreated PS.

The equilibrium contact angles were observed on these samples by using an optical microscope with in-built camera called the DinoCapture. Images were taken after water drops with the volumes of 7 to 10 μL were put on each sample. The advancing and receding contact angles, which are, respectively, the maximum and minimum values of equilibrium contact angles, are further measured on the samples by tilting the sample till the drop starts moving (Table 4-1). The experiment was recorded in the video form and then the image at the exact instance of slipping was captured and used to measure the advancing and receding contact angles. The values depicted on the images are the corresponding advancing angles and were reported after taking an average of 10 values for each sample.

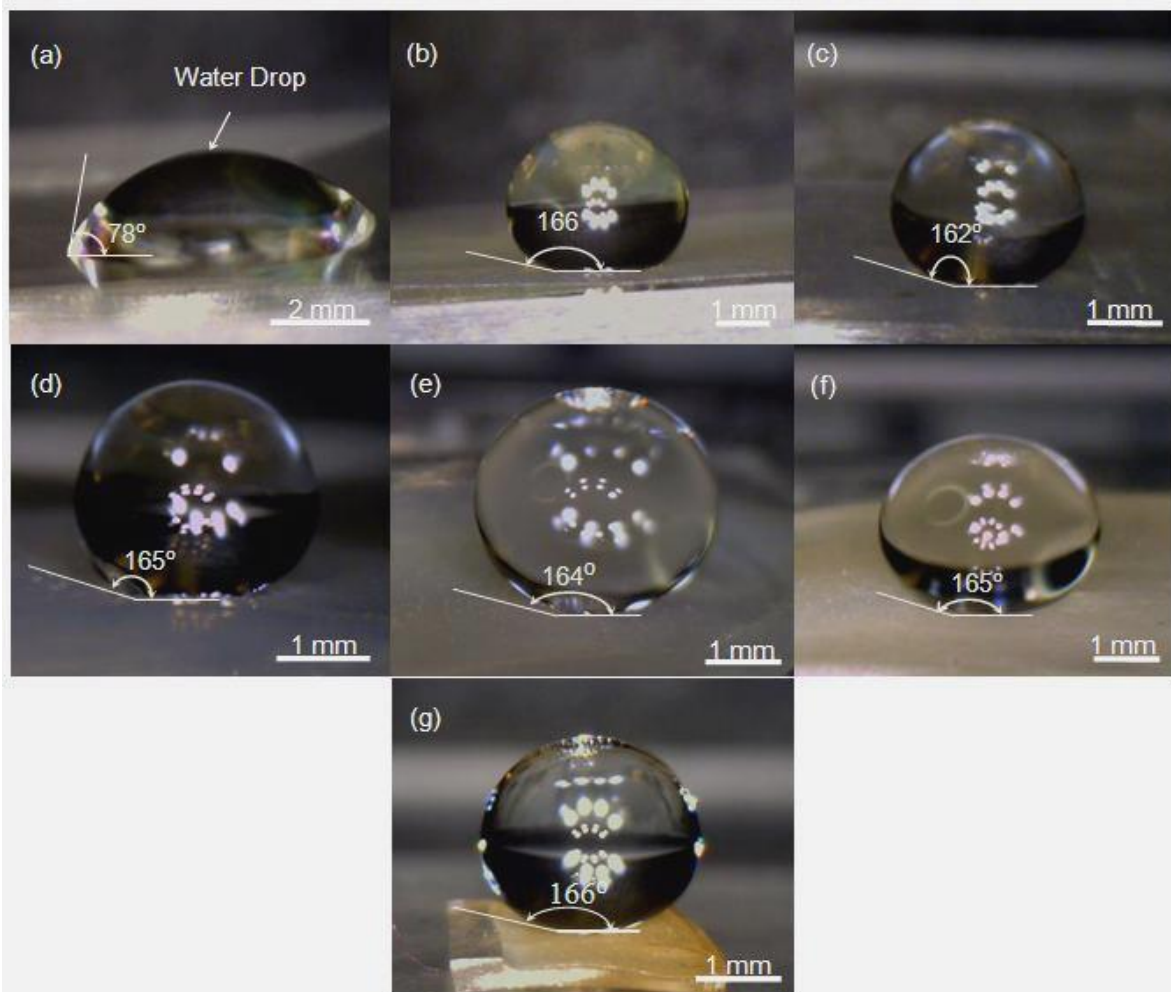


Figure 4-1: Contact angles of water drops on the surfaces with an error of $\pm 2^\circ$: (a) untreated PS, (b) Sample 1, (c) Sample 2, (d) Sample 3, (e) Sample 4, (f) Sample 5 and (g) Sample 6.

Table 4-1: Advancing contact angles, receding contact angles and contact angle measured experimentally, using an optical microscope.

Sample	$\theta_a \pm 2^\circ$	$\theta_r \pm 2^\circ$	$\theta_a - \theta_r \pm 2^\circ$
Untreated PS	78°	16°	62°
1	166°	150°	16°
2	162°	136°	26°
3	165°	151°	14°
4	164°	145°	19°
5	165°	144°	21°
6	166°	71°	95°

Two points are observed from the measured contact angles. First, the untreated PS sample has a hydrophilic surface, since even the corresponding advanced angle is below 90°. In contrast, due to the oxide layer and surface structures, all the six treated samples have superhydrophobic surfaces. Second, Sample 6 has the largest contact angle hysteresis of 95°, which is the difference between the advancing and receding contact angles, the untreated PS sample has the second largest of 62°, while the other samples have relatively small ones, which are less than 30°. A high contact angle hysteresis implies that the adhesion is high between a liquid drop and the corresponding surface [24]. Thus, this second point indicates that Sample 6 has the highest adhesion, and the other five treated samples have low adhesion.

4.2 Tilt Tests

Tilting tests were done on all the seven samples to examine whether water drops were easy to get away from the samples. This is another way to measure adhesion on a surface, as discussed in Introduction chapter, slip off of water drop at smaller angles will indicate low adhesion.

In such a test, a 10 μL water drop is first placed on a flat plate, on which a sample is fixed, and one end of the plate is then lifted up to find the minimum tilt angle of this plate for the water drop to roll or slide. If the minimum tilt angle is small, then it means that this water drop is easy to get off from the sample, and this sample has a low adhesion to water. As a consequence of the high adhesion on Sample 6, when this sample was rotated by 180° , a water drop still adhered to its surface (Figure 4-2(a)). On the other hand, when the tilt angles were larger than 30° , all the water drops have moved down on the other five treated samples (Figure 4-2(b)). Also, when the tilt angle was 50° , a water drop began to slide down on the untreated PS sample. The surface of Sample 6 is clearly superhydrophobic with high adhesion, which is similar to that of a rose petal [11], while those of the other five treated samples are superhydrophobic with low adhesion, which are close to that of a lotus leaf [1-10].

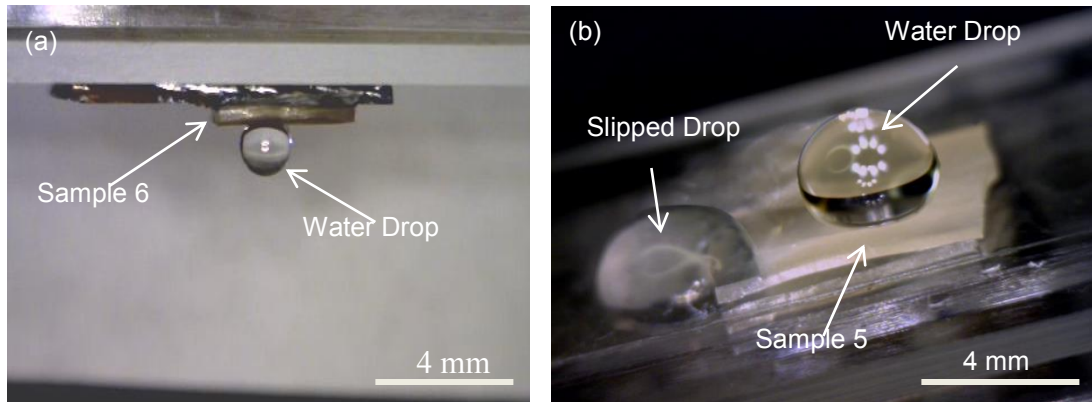


Figure 4-2: (a) A 10 μL water drop still hanged on Sample 6 when this sample was rotated by 180°. (b) Time lapse image of a 10 μL water droplet moving down the surface of Sample 5 at a tilt angle of 12°.

4.3 Roughness Factor Calculations

Wetting is dependent on the roughness values of a surface and to clearly investigate wetting states we will need to use roughness factor to decide which wetting state is exhibited by the different samples. In our case we have used the following equations to define r and f :

$$r = \text{Total area of a rough surface} / \text{The projected or planar area}, \quad (4-1)$$

$$f = \text{The area of the top of rough surface} / \text{The projected or planar area}, \quad (4-2)$$

These values were calculated for samples 1 to 5 by directly using their formulae and by assuming the surface structure atop them as frustum i.e a cone cut at the center. The total area considered for each sample was $5 \times 5 \mu\text{m}^2$. The top area was assumed to the area of a circle. The dimensions reported in Chapter 3, Figure 3-4 were utilized to

make estimations and calculate the r and f for each sample. Sample 6 was left out of this calculation due to its complex hybrid micro/nano structure.

Table 4-2: Values of r , f for sample 1-5 are tabulated.

Sample No.	r	f
1	1.4	0.03
2	2.4	0.02
3	2.5	0.02
4	4.9	0.02
5	5.1	0.026

Chapter 5

Results and Discussions

The samples 1-5 have similar type of microstructures atop their surfaces and are expected to exhibit similar wetting properties whereas Sample 6 is the hybrid micro/nano structures covered surface hence it will require for us to treat these two as separate cases and investigate their wetting phenomenon separately.

5.1 Wetting States of Samples 1-5

To explain the wetting properties measured on the six treated samples, we explored the wetting states on these samples. After water drops were put on Samples 1 to 5, we examined the interfaces between water drops and samples surfaces through side views using an optical microscope. Based on light reflection, we could see air gaps between the drops and the sample surfaces, indicating that the water drops were sitting on the tops of microhills or nanowires. Accordingly, the wetting on these five samples is in the Cassie-Baxter state [16]. In this state, we have [36],

$$\cos \theta_a = rf \cos \theta_c - 1 + f, \quad (5-1)$$

where θ_a represents the apparent contact angle obtained on the sample surface, θ_c denotes intrinsic contact angle of a liquid measured on a smooth plate, r is the roughness ratio of the wet surface area, and f is the fraction of solid surface area wet by the liquid, these values are calculated for samples 1-5 in Table 4-2. We treated a PS block for 10 s using ORIE, and used the corresponding contact angle measured as the value of θ_c . According to the dimensions of features measured on Samples 1 to 5, it follows from Eq. (4) that the values of θ_a on these samples are reported in Table 5-1.

Table 5-1: Values of intrinsic, experimental and theoretical contact angle for sample 1- 5.

Sample No.	$\theta_a \pm 2^\circ$	$\theta_a \pm 2^\circ$ (Experimental)	$\theta_a \pm 2^\circ$ (Theoretical)
1	78°	164°	166°
2	78°	165°	162°
3	78°	166°	165°
4	78°	163°	164°
5	78°	162°	165°

The inference of the Table 5-1 is that our experimental and theoretical values coincide and hence our prediction of Cassie Baxter wetting state was accurate.

However, it is not clear whether air gaps existed between a water drop and the surface of Sample 6 when the same light-reflection technique was applied to identify the wetting state. Hence, we adopted an alternative technique instead. As done previously in Ref. [36], we examined the wetting state through the top view using an optical microscope. As shown in Figure 5-1(a), after a 3 μ L water drop was added on Sample 6, the valleys between microwrinkles appeared dark, indicating that water completely filled these valleys. Meanwhile, the top portions of the microwrinkles were light, implying that air pockets were trapped between the water drop and microwrinkles. After a 1 μ L IPA solution was added to the water drop, as seen in Figure 5-1(b), the light-reflecting patches disappeared, meaning that the liquid mixture completely filled all the surface structures. A liquid drop fills all the roughness structures in a Wenzel state [16], while it

only sits on the top of all these structures in a Cassie-Baxter state [17]. Thus, as illustrated in Figure 5-2, according to the observed phenomena, the wetting on Sample 6 is considered to be a mixed state of Wenzel and Cassie-Baxter: water fills the valleys between microwrinkles, but not the gaps between the nanowires that are located on the top of the microwrinkles. The filling of these valleys makes a water drop get pinned on the surface. This wetting state is similar to what was observed on the surface of a rose petal [11].

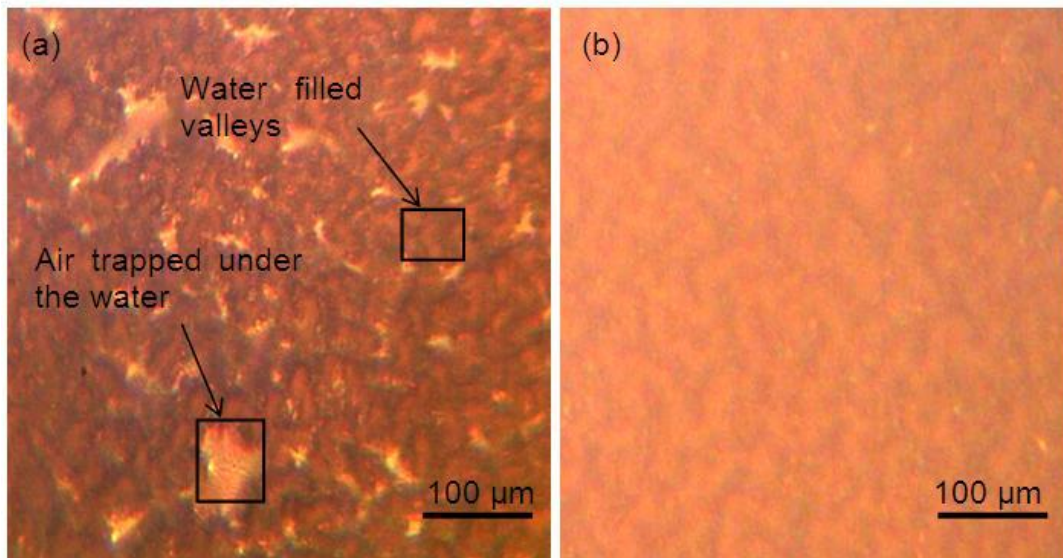


Figure 5-1: Optical images of Sample 6: (a) water filled valleys but not the top portions of the microwrinkles when a water drop was loaded on the sample surface and (b) addition of IPA to the water drop made the liquid also fill the top portions of the microwrinkles.

5.2 Wetting on Sample 6

We further explore why a mixed wetting state of Wenzel and Cassie-Baxter appears on the surface of Sample 6. In a previous work [37], we derived an angle inequality to judge whether a liquid drop filled the bottom corners of two microchannels:

$$360^\circ < (\theta_1 + \theta_2 + \varphi), \quad (5-2)$$

where θ_1 and θ_2 denote the apparent contact angles on the bottom and sidewall of the channel, respectively, and φ represents the inclination angle of the channel sidewall. Once this inequality is violated, the bottom corners of the channel are filled. Otherwise, they are not.

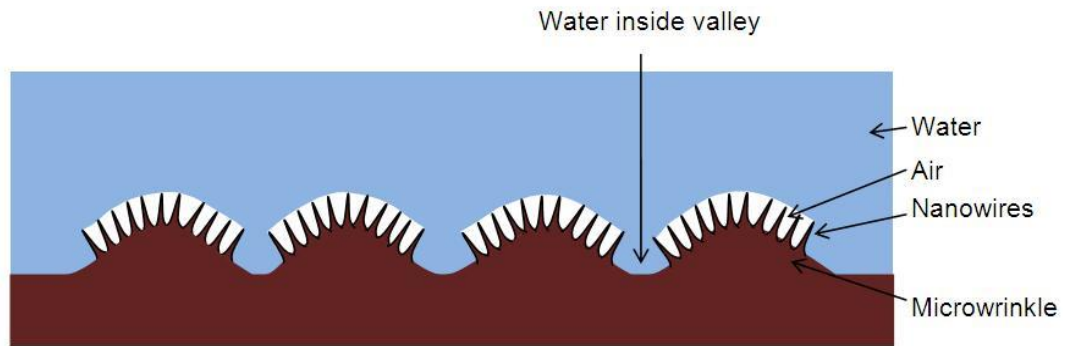


Figure 5-2: Schematic of a mixed state of Wenzel and Cassie-Baxter.

The inclination angles of the valley sidewalls of Sample 6 were measured to range from 26° to 30° (Figure 5-3). The valley between two microwrinkles may be approximated as a channel, and its sidewall and bottom are covered with nanowires. The apparent contact angles measured on Samples 2 to 5, which have nanowires-covered surfaces, are all less than 165° . Therefore, the values of both θ_1 and θ_2 are considered to be less than 165° as well. Accordingly, Ineq. (5-2) is violated, and water fills the valleys.

According to Ref. [38], in order for a liquid drop to fill the gap between two nanowires, the radius of a spherical liquid drop should be in the same order as or have a lower order than the pitch of the nanowires. The tested drop has a radius in the order of 1

mm. It is much larger than the pitch between two nanowires on Sample 6, which has the order of 100 nm. Hence, water did not fill the gaps between nanowires in our tests.

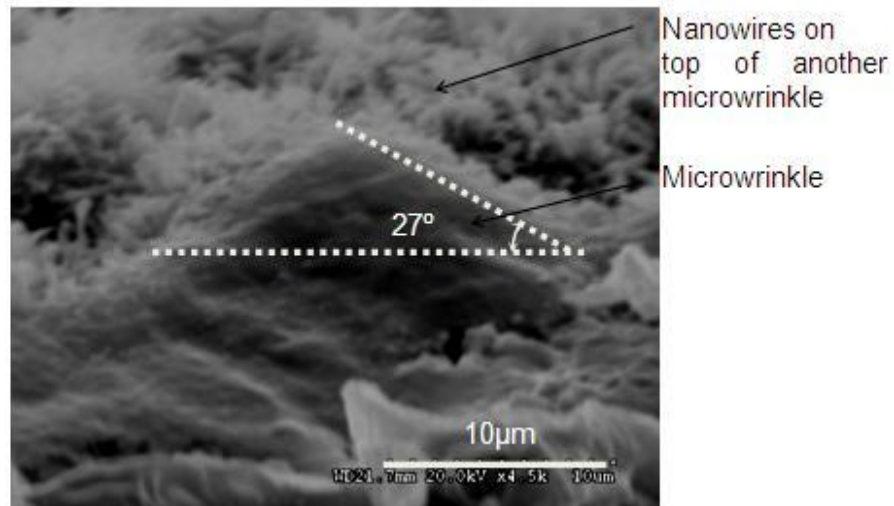


Figure 5-3: Cross-sectional (SEM) view of a microwrinkle (the nanowires on the microwrinkle were not seen, since the focus of the SEM was on the microwrinkle). The inclination angle of the microwrinkle was measured to be $27^{\circ} \pm 1^{\circ}$.

Chapter 6

Conclusions

In this work we have successfully demonstrated that simple surface modification of the PS using ORIE and variable strain-recovery temperature can generate surfaces that are superhydrophobic with tunable adhesion. The ORIE-treated PS blocks were recovered at temperatures ranging from 93°C to 162°C. The resulting samples all exhibited superhydrophobicity, and had advancing contact angles above 160°.

Out of the six samples; the first five samples have only microhills or nanowires on their surfaces. The corresponding wetting on the surface of each sample is in the Cassie-Baxter state, making a water drop easy to get off from this surface. Accordingly, these five samples have low adhesion to water.

On the other hand, Sample 6 has hybrid micro/nanostructures on its surface. The corresponding wetting is a mixed state of Wenzel and Cassie-Baxter. Although the advancing contact angle is high, the surface has high adhesion to a water drop. The presented results indicate that, through simple control of the strain-recovery temperature, samples can have different surface structures for either lotus- or petal-like wetting applications.

They may prove important in development of devices that can use their tunability to the maximum potential in the fields of micro-fluidics, biomedical applications and lab on a chip devices. The advantages of these samples are a lot and to name a few, they are cost efficient, environmentally stable, and biodegradable. They are simple to fabricate. The samples are all made from the same material PS and apart from recovery temperature rest all the parameters have been maintained to be similar. This particular

surface modification of PS holds a bright future in the studies and applications related to superhydrophobicity.

References

- [1] Neinhuis C, Barthlott W 1997 Characterization and distribution of water-repellent, self-cleaning plants surfaces *Annals of Botany* 79 667-677
- [2] Zhu L, Xiu Y, Xu J, Tamirisa P A, Hess D W, Wong C 2005 Superhydrophobicity on two-tier rough surfaces fabricated by controlled growth of aligned carbon nanotube arrays coated with fluorocarbon *Langmuir* 21 11208-11212
- [3] Ming W, Wu D, Benthem van R, de With G 2005 Superhydrophobic films from raspberry-like particles, *Nano Letters* 5 2298-2301
- [4] Zhang Y, Sundararajan S 2008 Superhydrophobic engineering surfaces with tunable air- tapping ability *Journal of Micromechanics and Microengineering* 18 035024-7
- [5] Choi S J, Suh K Y, Lee H H A geometry controllable approach for the fabrication of biomimetic hierarchical structure and its superhydrophobicity with near-zero sliding angle 2008 *Nanotechnology* 19 275305-5
- [6] Bhushan B, Koch K, Jung Y C Fabrication and characterization of the hierarchical structure for superhydrophobicity and self-cleaning 2009 *Ultramicroscopy* 109 1029-1034
- [7] Koch K, Bhushan B, Jung Y C, Barthlott W Fabrication of artificial lotus leaves and significance of hierarchical structure for superhydrophobicity and low adhesion 2009 *Soft Matter* 5 1386-1393
- [8] Wang J, Chen H, Sui T, Li A and Chen D Investigation on hydrophobicity of lotus leaf: experiment and theory 2009 *Plant Science* 176 687-695
- [9] Xiang M, Wilhelm A and Luo C Existence and role of large micropillars on the leaf surfaces of the president lotus 2013 *Langmuir* 29 7715-7725

- [10] Feng L, Zhang Y, Xi J, Zhu Y, Wang N, Xia F, Jiang L 2008 Petal effect: a superhydrophobic with high adhesive force, *Langmuir* 24 4114-4119
- [11] Bhushan B, Nosonovsky M The rose petal effect and the modes of superhydrophobicity 2010 *Phil. Trans. R. Soc. A* 368 4713-4728
- [12] Karaman M, Ç abuk N, Özyurt D, Köysüren Ö Self-supporting superhydrophobic thin polymer sheets that mimic the nature's petal effect 2012 *Applied Surface Science* 259 542-546
- [13] Sharfrin E, Zisman W A Constitutive relations in the wetting of low energy surfaces and the theory of the retraction method of preparing monolayers 1960 *The Journal of Physical Chemistry* 64 519-524
- [14] Young T An essay on the cohesion of fluids 1805 *Phil.Trans.R.Soc.London* 95 65-87
- [15] Dupre' A *Theorie Mechanique de la Chaleur* 1869 Gauthier- Villars Paris 369ff
- [16] Wenzel R N Resistance of solid surfaces to wetting by water 1936 *Ind. Engg. Chem.* 28 988-994
- [17] Cassie A B D and Baxter S Wettability of porous surfaces 1944 *Trans. Faraday Soc.* 40 546
- [18] Hu J, Zhu Y, Huang H and Lu J Recent advances in shape-memory polymers: structures, mechanism, functionality, modeling and applications 2012 *Progress in Polymer Science* 37 1720-1763
- [19] Wang C C, Huang W M, Ding Z, Zhao Y and Purnawali H Cooling-/water-responsive shape memory hybrids 2012 *Compos. Sci. Technol.* 72 1178-1182
- [20] Hidber P, Nealey P, Helbig W and Whitesides G New strategy for controlling the size and shape of metallic features formed by electroless deposition of copper:

microcontact printing catalysts on oriented polymers, followed by thermal shrinkage 1996 *Langmuir* 12 5209-5215

- [21] Zhao X, Xia Y, Schueller O, Qin D and Whitesides G Fabrication of microstructures using shrinkable polystyrene films 1998 *Sensors and Actuators A* 65 209-217
- [22] A. Grimes, D. Breslauer, M. Long, J. Pegan, L. Lee and M. Khine Shrinky- dink microfluidics: rapid generation of deep and rounded patterns 2008 *Lab on a Chip* 8 170-172
- [23] K. Gall, P. Kreiner, D. Turner and M. Hulse Shape-memory polymers for microelectromechanical systems 2004 *Journal of Microelectromechanical Systems* 13 472-483
- [24] Fu C C, Grimes A, Long M, Ferri C, Rich B, Ghosh S, Ghosh S, Lee L and Gopinathan A, Khine M Tunable Nanowrinkles on Shape Memory Polymer Sheets 2009 *Advanced Materials* 21 4472-4476
- [25] Sun L, Zhao Y, Huang W M and Tong T H Formation of combined surface features of protrusions array and wrinkles atop a shape-memory polymer 2009 *Surface Review and Letters* 16 929-933
- [26] Zhao Y, Huang W M and Fu Y Q Formation of micro/nano-scale wrinkling patterns atop shape memory polymers 2011 *Journal of Micromechanics and Microengineering* 21 067007
- [27] Liu X, Chakraborty A and Luo C Fabrication of micropatterns on the sidewalls of a thermal shape memory polystyrene block 2010 *Journal of Micromechanics and Microengineering* 20 095025

- [28] Chakraborty A, Liu X C and Luo C Generation of sidewall patterns in microchannels via strain recovery deformations of polystyrene 2012 *Sensor. Actuat. a-Phys.* 188 374-382
- [29] Chakraborty A, Xiang M and Luo C Fabrication of super-hydrophobic microchannels via strain-recovery deformations of polystyrene and oxygen reactive ion etch 2013 *Materials* 6 3610-3623
- [30] Luo C, Liu X C, Poddar R, Garra J, Gadre A P, Keuren E V, Schneider T, White R, Currie J and Paranjape M Thermal ablation of PMMA for water release using a microheater 2006 *J. Micromech. Microeng.* 16 580-588
- [31] Guruvenket S, Rao G M, Komath M and Raichur A M Plasma surface modification of polystyrene and polyethylene 2004 *Applied Surface Science* 236 278-284
- [32] Occhiello E, Morra M, Cinquina P and Garbassi F Hydrophobic recovery of plasma treated polystyrene 1992 *Polymer* 33 3007
- [33] Park J, Chae H Y, Chung C, Sim S J, Park J, Lee H H and Yoo P J Controlled wavelength reduction in surface wrinkling in poly(dimethylsiloxane) 2010 *Soft Matter* 6 677-684
- [34] Groenewold J Wrinkling of plates coupled with soft elastic media 2001 *Physica A* 298 32-45
- [35] Bowden N, Brittain S, Evans A, Hutchinson J and Whitesides G Spontaneous formation of ordered structures in thin films of metals supported on an elastomeric polymer 1998 *Nature* 393 146-149
- [36] Teisala H, Tuominen M and Kuusipalo J Adhesion mechanism of water droplets on hierarchically rough superhydrophobic rose petal surface 2011 *Journal of Nanomaterials* Article ID 818707

- [37] Luo C, Xiang M and Heng X A stable intermediate wetting state after a water drop contacts the bottom of a microchannel or is placed on a single corner 2012 Langmuir 28 9554-61
- [38] Jung Y C and Bhushan B Wetting transition of water droplets on superhydrophobic patterned surfaces 2007 Scripta Mater. 57 1057-1060

Biographical Information

Prasha Sarwate has received a Bachelor's of Engineering Degree in Chemical Engineering from Vishwakarma Institute of Technology (V.I.T), Pune University, India in July 2011. During her undergraduate studies she worked on metal matrix composites, and fabricated a set up that can help increase the tensile strength of the alloy by effectively dispersing the SiC particles, the alloy was specifically designed for mechanical or aerospace applications. She was the founder member of various organizations on campus and worked with fellow students to discover new projects and interesting challenges. She also participated as the design head for the team that represented V.I.T at SAE Aero Design West 2011, Texas USA, and the team received three awards, including the best overall performance. She also worked on a start- up company called Aircraft as the founder and director for a year and a half. During this time she organized 20 plus workshops for 350 plus engineering students.

She has been a Graduate student in the Mechanical & Aerospace Engineering Department at UTA since August 2012. She joined Dr.Cheng Luo's group in October 2012 and worked with his group on projects related to shape memory polymers and their wetting properties. Her interests are majorly, project management, micro/electro mechanical systems, mechanical designing, and development of new age surface modifications or coatings using polymers which are more efficient. She has been selected by General Cable, a fortune 500 company for their Engineering Technology Program, which she will be joining full time starting from the summer of 2014.